PHYSICAL REVIEW FLUIDS **1**, 081501(R) (2016)

Reynolds number dependence of large-scale friction control in turbulent channel flow

Jacopo Canton,[1,2,*] Ramis Örlü,[1] Cheng Chin,[3] and Philipp Schlatter[1,2]
[1]*Linné FLOW Centre KTH Mechanics, Royal Institute of Technology, Stockholm, SE-100 44, Sweden*
[2]*Swedish e-Science Research Centre (SeRC)*
[3]*The University of Adelaide, Department of Mechanical Engineering, Adelaide, South Australia 5005, Australia*

(Received 13 October 2016; published 27 December 2016)

The present work investigates the effectiveness of the control strategy introduced by Schoppa and Hussain [Phys. Fluids **10**, 1049 (1998)] as a function of Reynolds number (Re). The skin-friction drag reduction method proposed by these authors, consisting of streamwise-invariant, counter-rotating vortices, was analyzed by Canton *et al.* [Flow, Turbul. Combust. **97**, 811 (2016)] in turbulent channel flows for friction Reynolds numbers (Re_τ) corresponding to the value of the original study (i.e., 104) and 180. For these Re, a slightly modified version of the method proved to be successful and was capable of providing a drag reduction of up to 18%. The present study analyzes the Reynolds number dependence of this drag-reducing strategy by performing two sets of direct numerical simulations (DNS) for $\mathrm{Re}_\tau = 360$ and 550. A detailed analysis of the method as a function of the control parameters (amplitude and wavelength) and Re confirms, on the one hand, the effectiveness of the large-scale vortices at low Re and, on the other hand, the decreasing and finally vanishing effectiveness of this method for higher Re. In particular, no drag reduction can be achieved for $\mathrm{Re}_\tau = 550$ for any combination of the parameters controlling the vortices. For low Reynolds numbers, the large-scale vortices are able to affect the near-wall cycle and alter the wall-shear-stress distribution to cause an overall drag reduction effect, in accordance with most control strategies. For higher Re, instead, the present method fails to penetrate the near-wall region and cannot induce the spanwise velocity variation observed in other more established control strategies, which focus on the near-wall cycle. Despite the negative outcome, the present results demonstrate the shortcomings of the control strategy and show that future focus should be on methods that directly target the near-wall region or other suitable alternatives.

DOI: 10.1103/PhysRevFluids.1.081501

The search for an effective mean of reducing turbulent skin-friction drag is one of the most active fields of research in fluid mechanics. The benefits of efficient flow control are numerous: from energy and economical savings, to more efficient and greener machinery, be it aviation or fluid transport and mixing [1]. Several techniques have been investigated, ranging from passive methods such as riblets [2] to active control strategies as, for example, streamwise-traveling waves of blowing and suction [3,4]; of spanwise wall velocity [5], or of wall deformation [6]; oscillating walls [7,8]; uniform blowing and suction [9]; volume forcing [10]; and direct modification of the mean flow [11]. Most of these control techniques, though, have been analyzed only at low Reynolds numbers (Re) and only recently some authors have started investigating the effects that an increasing Reynolds number has on the flow control strategy (see, for instance, Iwamoto *et al.* [12], Hurst *et al.* [13], and Gatti and Quadrio [14]).

One of the more prominent techniques consists in the large-scale vortices proposed by Schoppa and Hussain [11], which (in the original study) were embedded in a turbulent channel flow at a friction Reynolds number $\mathrm{Re}_\tau = 104$, where turbulence is marginally sustainable. This drag reduction (DR)

*jcanton@mech.kth.se

TABLE I. Details of the numerical discretization employed for the present simulations. T corresponds to the duration of the controlled simulations; N_x and N_z represent the number of Fourier modes employed in the wall-parallel directions (values before de-aliasing), while N_y is the order of the Chebyshev expansion used for the wall-normal direction.

Re_τ	Integration time $T \cdot [h/U_b]$	Domain size $L_x/h,\ L_z/h$	Grid points $N_x,\ N_y,\ N_z$
104	10500	8, 3.832	48, 65, 48
		8, 6.6	48, 65, 60
		8, 9.9	48, 65, 96
180	1500	12, 6.6	128, 97, 96
		12, 9.9	128, 97, 144
360	1000	12, 6.6	300, 151, 200
		12, 9.9	300, 151, 300
550	400	12, 6.6	432, 193, 300

strategy was found to be ineffective by Canton *et al.* [15], since the claimed drag reduction effect was shown to be of transient nature. Nonetheless, Canton *et al.* [15] recast the method as a volume forcing control for channel flows that lead to sustainable drag reduction at $\mathrm{Re}_\tau = 180$. These large-scale vortices had been promoted by their original authors as a promising, feed-forward, or passive control technique capable of reducing the turbulent friction drag from the outside of the viscous layer, and thus independent of the small scales of wall turbulence, which would otherwise limit its applicability at practically relevant Reynolds numbers due to sensor and actuator limitations [16]. The vortices would do so by reducing the wall-normal vorticity ω_y, therefore preventing streak instability and generation of streamwise vortices [11].

It is well known, though, that near-wall structures scale with viscous units (see, e.g., the seminal paper by Kline *et al.* [17]) and that low Reynolds number effects are present in wall-bounded flows at least up to $\mathrm{Re}_\tau = 395$ [18]. Moreover, it has been found that the performance of different control strategies deteriorates as the Reynolds number is increased; this is the case at least for the active V- and suboptimal control schemes by Iwamoto *et al.* [12] and the oscillating wall and traveling waves by Hurst *et al.* [13] and Gatti and Quadrio [14,19]. These two observations provide the main motivation for the present analysis, along with the aim of better characterizing the large-scale vortex control.

This paper is concerned with direct numerical simulations (DNS) of incompressible channel flows at fixed bulk Reynolds number Re_b, based on bulk velocity U_b, channel half-height h, and fluid viscosity ν. Four values of bulk Reynolds number are employed: $\mathrm{Re}_b = 1518$, 2800, 6240, and 10 000, such as to result in a friction Reynolds number, based on friction velocity u_τ, h, and ν, corresponding to $\mathrm{Re}_\tau \approx 104$, 180, 360, and 550, where the lowest Reynolds number corresponds to the value employed in the original study by Schoppa and Hussain [11]. The simulations are performed using the fully spectral code SIMSON [20], where periodicity in the wall-parallel directions x (streamwise) and z (spanwise) is imposed, and the no-slip and no-penetration conditions are applied at the two channel walls. The wall-parallel directions are discretized using Fourier series, where aliasing errors are removed by using 3/2 times the number of modes prescribed. A Chebyshev expansion is employed in the wall-normal direction y. Details of the domain sizes and spatial resolutions used for the four sets of simulations are reported in Table I. The temporal discretization of the nonlinear term is carried out by a four-stage Runge-Kutta scheme, while the linear terms are treated with a second-order Crank-Nicolson scheme. The time step is automatically set such that the Courant number is always below 0.8.

The simulations are initialised with a randomly perturbed Poiseuille velocity profile. A precursor run is performed with the control turned off until a statistically steady, thus fully turbulent, flow is obtained. All controlled simulations are then initialized with the same snapshot from the uncontrolled

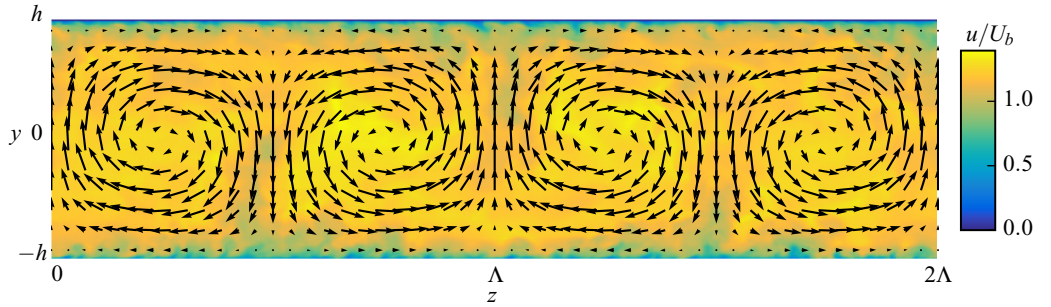

FIG. 1. Instantaneous flow field of a controlled simulation for $\mathrm{Re}_\tau = 550$ illustrating the large-scale vortices. The figure depicts two vortex wavelengths, with $\Lambda = 3.3h$, on a cross-stream channel plane colored by streamwise velocity magnitude. The control amplitude is $\max|\langle v\rangle_{x,t}| \approx 0.07U_b$.

case. The controlled simulations are run for a sufficiently long-time interval such as to have a reasonably low uncertainty on the statistical quantities presented in this work and, in particular, on the value of drag reduction (see, e.g., Fig. 2, which presents the error bars on DR). For additional details, see Canton *et al.* [15] and Table I. The large-scale vortices, provided with variable intensity and spanwise wavelength, are imposed via a volume forcing defined as [11]

$$\begin{aligned} f_x &= 0, \\ f_y(y,z) &= A\beta\cos(\beta z)[1+\cos(\pi y/h)], \\ f_z(y,z) &= A\pi/h\sin(\beta z)\sin(\pi y/h), \end{aligned} \tag{1}$$

where A is the forcing amplitude and β is the wave number along z. The wave number was chosen such as to have vortex periods $\Lambda = 2\pi/\beta$ between $1.1h$ and $9.9h$, corresponding to inner-scaled wavelengths Λ^+ between 120 and 3630. Here and in the following, all inner-scaled quantities are referred to the uncontrolled case and are indicated with a plus sign, i.e., $(\cdot)^+$. A sketch of the control vortices for $\Lambda = 3.3h$ is depicted in Fig. 1. Since A does not correspond to a measurable flow quantity, the maximum wall-normal mean velocity is used to characterize the strength of the vortices, i.e., $\max|\langle v\rangle_{x,t}|/U_b$, where $\langle\cdot\rangle_{x,t}$ denotes the average in the streamwise direction and time.

The present vortex control is a good candidate for practical implementation: The required large-scale secondary flow can in fact be generated by using either active or passive control methods that do not require any moving parts. Examples of such methods include, but are not limited to, modifying the surface geometry by introducing vortex generators [21], or nonuniform surface roughness [22], exploiting flow instabilities [23], as well as employing plasma streamwise vortex generators [24,25].

Here, drag reduction is quantified as the relative difference in the time-averaged streamwise pressure gradient p_x, necessary to fix the mass flux, between controlled $p_{x_{\mathrm{con}}}$ and uncontrolled $p_{x_{\mathrm{unc}}}$ flow cases:

$$\mathrm{DR} = \frac{p_{x_{\mathrm{unc}}} - p_{x_{\mathrm{con}}}}{p_{x_{\mathrm{unc}}}}. \tag{2}$$

Clearly, positive values correspond to a favorable effect while negative DR indicates drag increase. Note that this definition of DR, in the case of a turbulent channel flow, corresponds also to the same ratio between controlled and uncontrolled average wall-shear stress.

The uncertainty on DR is quantified as [26]

$$\sigma^2_{\langle\mathrm{DR}\rangle} = \frac{1}{T}\int_{-T}^{T}\left(1-\frac{|\tau|}{T}\right)C_{\mathrm{DR\,DR}}(\tau)d\tau, \tag{3}$$

where $C_{\mathrm{DR\,DR}}(\tau)$ is the autocovariance of DR, and T is the length of the integration time (see Table I).

A total of 222 controlled simulations have been performed varying the Reynolds number, the control amplitude, and the wavelength of the vortices. As shown by Canton *et al.* [15], the control

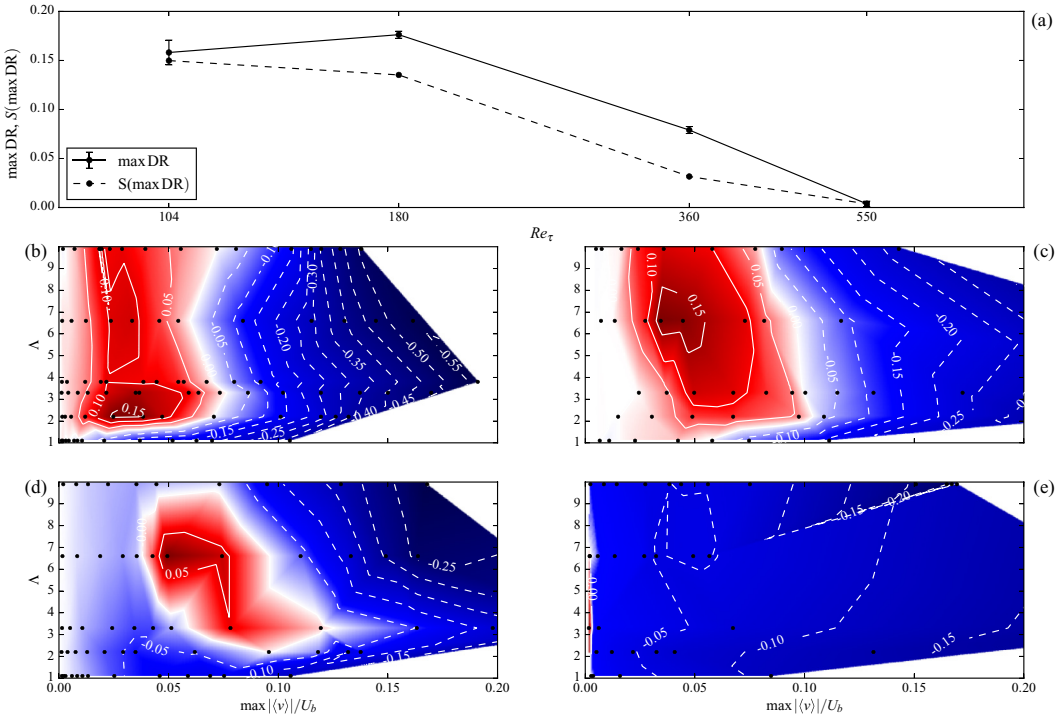

FIG. 2. Panel (a): maximum achievable drag reduction as a function of friction Reynolds number (continuous line) and corresponding net power saving (dashed line). The uncertainty of DR is quantified by Eq. (3); the x axis is in logarithmic scale. Panels (b) to (e) depict DR as a function of control strength, $\max|\langle v\rangle_{x,t}|/U_b$, and wavelength of the vortices, Λ. $\mathrm{Re}_\tau = 104, 180, 360$, and 550 are reported in panels (b)–(e), respectively. In panels (b)–(e) red and blue colors correspond to interpolated positive, respectively negative, values (reported as labels on the isocontours) of DR, based on the simulations indicated through black points.

scheme is effective at both $\mathrm{Re}_\tau = 104$ and 180. For these values of the Reynolds number, drag reductions of up to 16% and 18%, respectively, can be achieved. The performance of the large-scale vortices, though, degrades rapidly: for $\mathrm{Re}_\tau = 360$ the maximum DR is only 8%, and for $\mathrm{Re}_\tau = 550$ no more than $0.4\% \pm 0.28\%$ can be obtained. It should be noted that, as detailed in the following, the present analysis covers the entire range of control amplitudes and reasonable vortex wavelengths. The drag reduction values presented are, therefore, the highest achievable under optimal conditions. This result is in good agreement with the work by Fukagata *et al.* [27], who found that selectively damping small-scale velocity fluctuations in a turbulent channel flow for $\mathrm{Re}_\tau = 640$ is more effective than damping their large-scale counterparts, albeit their control targeting the large-scale structures is different from the following approach based on Shoppa and Hussain [11].

The drag reduction including its uncertainty is illustrated in Fig. 2 where Fig. 2(a) (in semilog scale) shows the maximum achievable value of DR as a function of the Reynolds number. Figures 2(b)–2(e) show the details at each Reynolds number by presenting the performance of the control strategy for $\mathrm{Re}_\tau = 104, 180$, and 360 as a function of forcing amplitude and vortex wavelength. It can be observed that the forcing amplitude for optimal drag reduction remains relatively low even as the Reynolds number increases, varying between $\max|\langle v\rangle_{x,t}|/U_b = 0.025$ and 0.049 for Re_τ between 104 and 360.

The optimal wavelength, instead, is affected more significantly, at least for low Reynolds numbers. Analyzing its dependence on Re in outer scaling, the optimal Λ is $2.2h$ for $\mathrm{Re}_\tau = 104$. This increases to $\Lambda = 6.6h$ for $\mathrm{Re}_\tau = 180$, which appears to be the optimal value for $\mathrm{Re}_\tau = 360$ as well. For $\mathrm{Re}_\tau = 550$, however, no drag reduction can be achieved for any amplitude of control

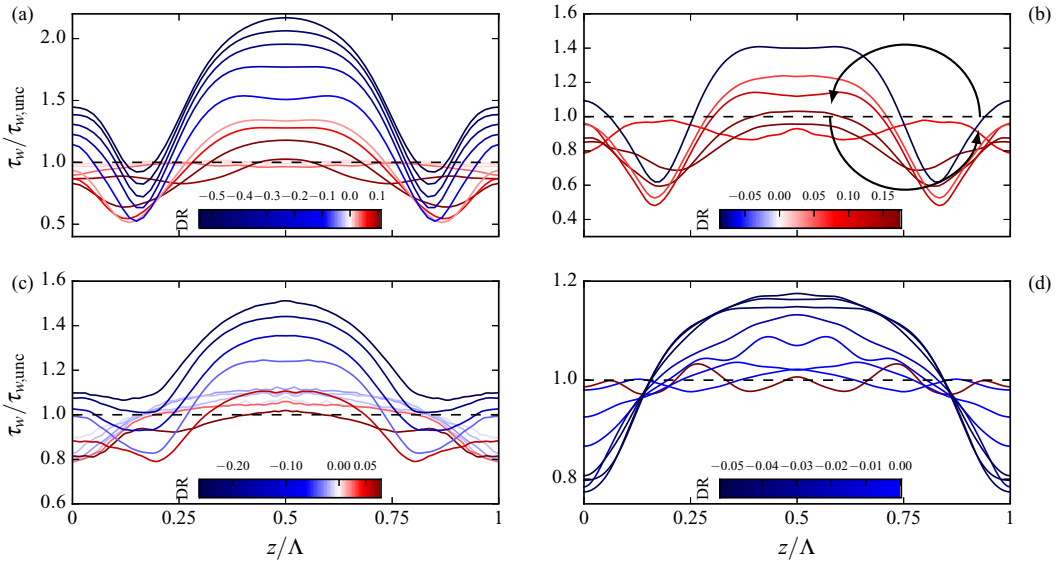

FIG. 3. Wall shear stress at the lower channel wall ($y = -1$) normalized by the corresponding value in the uncontrolled case ($\tau_w = 1$). Each line corresponds to a different forcing amplitude. The vortices are pushing fluid towards the wall at $z/\Lambda = 0.5$ while lifting it at $z/\Lambda = 0$ and 1, as indicated by the arrows in panel (b) which indicate the spanwise location and direction of the vortices. The four panels (a)–(d) correspond to increasing Reynolds numbers, $\mathrm{Re}_\tau = 104, 180, 360$, and 550, and show the measurements for control vortices with $\Lambda = 6.6h$. A similar picture is observed for the other wavelengths investigated. The curves are color-coded with their value of DR, reported in the legends. The dark red line in panel (d) corresponds to a drag reduction of only 0.02%, the highest achievable value for $\mathrm{Re}_\tau = 550$ for vortices with $\Lambda = 6.6h$.

vortices with $\Lambda = 6.6h$. When scaled in inner units, instead, the optimal wavelength Λ^+ increases with friction Reynolds number, growing from $\Lambda^+ = 232$ for $\mathrm{Re}_\tau = 104$ to 1205 and 2415 for $\mathrm{Re}_\tau = 180$ and 360, respectively. Extrapolating this trend in inner units to $\mathrm{Re}_\tau = 550$, the optimal Λ^+ value would be around 3500. Simulations for this Reynolds number, though, controlled with vortices of wavelength equal to $6.6h$, corresponding to $\Lambda^+ = 3600$, do not exhibit drag reduction for any forcing amplitude. To further verify that the size of the control vortices does not scale in inner units, simulations with two rows of circular vortices were also performed for $\mathrm{Re}_\tau = 180$. The two rows were placed close to the two channel walls and featured vortices with $\Lambda = 1.1h$ and different forcing amplitudes. Also this implementation of the control scheme could only provide drag increase.

Since the method under investigation is an active control scheme, the power used to generate and sustain the large-scale vortices needs to be taken into account for a complete assessment of the performance. The net power saving rate is defined as $S = (P_{\mathrm{unc}} - P_{\mathrm{con}})/P_{\mathrm{con}} = \mathrm{DR} - P_{\mathrm{in}}/P_{\mathrm{unc}}$ (see, for instance, Gatti and Quadrio [14]), where P_{unc} is the power required to drive the uncontrolled channel flow, while P_{in} is the power needed by the control, computed for an ideal actuator as $P_{\mathrm{in}} = 1/(\Omega T)\int_\Omega \int_0^T \boldsymbol{f}\cdot\boldsymbol{v}\,\mathrm{d}t\,\mathrm{d}\Omega$. As can be observed in Fig. 2(a), the Reynolds number dependence of this figure of merit is qualitatively similar to that of DR, confirming that the large-scale vortices perform well for low Reynolds numbers but fail to provide a positive effect for $\mathrm{Re}_\tau > 550$. In particular, it was observed that the energy consumed by the ideal actuators does not significantly affect the parameters for the control: Both the optimal wavelength and the forcing amplitude exhibit the same values compared to when not considering the power used to generate the large-scale vortices.

Valuable insight on the Reynolds number effect on the large-scale vortices can be obtained by analyzing the wall-shear stress as a function of Re_τ. Figure 3 presents the profiles of τ_w, normalized by the value of the uncontrolled case, measured at the lower channel wall ($y = -1$) for the four investigated Re_τ values. The analysis is conducted on vortices with $\Lambda = 6.6h$ which better highlight

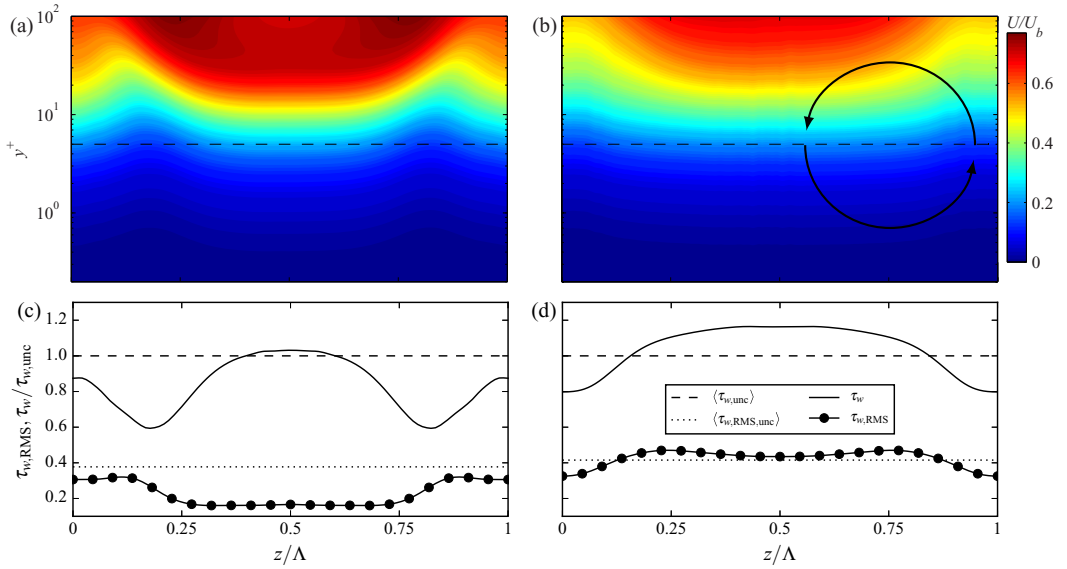

FIG. 4. Average streamwise velocity on a cross-stream (i.e., spanwise and wall-normal) plane (a),(b) and corresponding wall-shear stress and fluctuations on the lower channel wall (c),(d), normalized by the average wall-shear stress of the uncontrolled case. Two cases are depicted for friction Reynolds numbers $\mathrm{Re}_\tau = 180$ (a),(c) and $\mathrm{Re}_\tau = 550$ (b),(d). In both cases the flow is controlled with large-scale vortices with $\Lambda = 6.6h$ and $\max|\langle v\rangle_{x,t}| \approx 0.05U_b$. It can be observed that the control vortices can only barely penetrate the viscous sublayer (highlighted with a dashed line at $y^+ = 5$) for the higher Re_τ. Moreover, while in panels (a),(c) the flow is significantly laminarized in the region where fluid is pushed towards the wall ($0.25 < z/\Lambda < 0.75$), the opposite is observed in panels (b),(d). The arrows in panel (b) indicate the spanwise location and direction of the vortices.

the Reynolds number dependence, but the same trend is observed for all other wavelengths. Two phenomena are clearly observable as the Reynolds number is increased: a reduction in the fluctuation amplitude of τ_w and a modification of the profiles as a function of z.

The first phenomenon is most probably a direct consequence of the increase in Reynolds number: As Re_τ is increased the height of the viscous sublayer, measured in outer units, decreases as $1/\mathrm{Re}_\tau$. The maximum variation in τ_w (for a positive DR) at the center of two vortices, where the fluid is pushed towards the wall, does also decrease monotonically with Re_τ. This may explain why the large-scale vortices cannot penetrate the viscous sublayer as its height decreases, as will become apparent in the comparison in Fig. 4, and thus cannot affect the near-wall region as Re_τ is increased beyond a limit value.

The second phenomenon is well illustrated by comparing Figs. 3(a) and 3(b) with Figs. 3(c) and 3(d), although it is also apparent in Fig. 3(c) alone. For controlled flows at low Reynolds numbers the minimum in τ_w is achieved close to the vertical vortex axes, at $z/\Lambda \approx 0.16, 0.84$; in this area the vortices are pushing the fluid parallel to the wall, similarly to spanwise traveling waves, which are a proven drag reduction strategy [28]. As the Reynolds number is increased, this minimum is moved to the extrema of the period, where the vortices are lifting the fluid away from the wall [see Fig. 3(d)]. Concurrently, the area where the wall-shear stress is increased becomes wider than $\Lambda/2$, extending over the vertical vortex axes. The most relevant modification takes place at $z/\Lambda = 0$ and 1, where the vortices are lifting fluid from the wall: For low Reynolds numbers this region is characterized by an increase in τ_w, while for high Re_τ the wall-shear stress is significantly reduced, similar to what is observed in control via mass injection (i.e., blowing) [9]. These modifications are clear at the intermediate $\mathrm{Re}_\tau = 360$ [Fig. 3(c)] where both low and high Reynolds number profiles of τ_w can be observed.

For $\mathrm{Re}_\tau = 550$ both phenomena are observable: The drag is increased even by vortices with very small amplitude, and all forcing amplitudes that have a sensible effect on the flow increase the drag over more than 3/4 of the domain.

If the first of these phenomena can be easily attributed to an increase of Re_τ alone, and only results in a decrease in amplitude, the modification of the τ_w profiles is an indication of a more fundamental change in the flow mechanics affected by the large-scale vortices. A third fundamental effect that the Reynolds number has on this drag-reduction strategy concerns relaminarization. It was observed by Canton *et al.* [15] that the large-scale vortices induce relaminarization for $\mathrm{Re}_\tau = 104$ and 180 in the region where fluid is pushed towards the wall [see Fig. 4(c)]. The opposite effect is observed for $\mathrm{Re}_\tau = 550$. For this Reynolds number the RMS of the wall-shear stress is actually increased where the vortices push fluids towards the wall and decreased in the upwelling regions [see Fig. 4(d)]. The reason for this perhaps unexpected behavior can probably be connected to the reducing effect that the flow control has on the near-wall region when the Reynolds number is increased. For the lower Reynolds numbers the streaks reach the near-wall region and accelerate the flow in the down-draft areas; this, in turn, renders the near-wall region more stable and thus leads to laminarization. On the other hand, when the streaks do not reach down into the near-wall region (at higher Re), the main effect is a vertical compression of the near-wall layer, which increases the overall gradient and thus promotes more instabilities, consequently increasing the fluctuations in the wall-shear stress.

To summarize, results show that the large-scale vortices can provide considerable drag reduction for low Reynolds numbers but their performance decreases rapidly and the method becomes completely ineffective by $\mathrm{Re}_\tau = 550$. Clearly, low Reynolds number effects are still present for $\mathrm{Re}_\tau = 104, 180$ [18] and the present large-scale control is able to affect the low-Re wall cycle and to reduce the turbulence intensity. $\mathrm{Re}_\tau = 360$ offers a good transitional flow case, close to $\mathrm{Re}_\tau = 395$, which was observed by Moser *et al.* [18] as being a good lower limit for the absence of low Reynolds number effects. For this Reynolds number, in fact, both the low and high Re behavior of the large-scale vortices can be observed. For higher Reynolds numbers the low Re effects disappear and the present control strategy cannot provide drag reduction anymore. The effect of the vortices on the flow is also changed: While for low Re the maximum reduction in wall-shear stress is achieved via spanwise variation of the flow, for high Re it is obtained via a 'blowing' mechanism. Despite the negative overall outcome, these results offer ideas upon which to improve the control strategy: The vortices can reduce τ_w for high Reynolds numbers in the upwelling regions [see Fig. 3(d)]. A control strategy capable of generating such wall jets, without creating a large area of drag increase, would have an overall positive effect on DR. Moreover, a technique capable of generating fluid lift up directly at the wall, unlike the present one based on motion created outside of the viscous layer, would probably be more successful for high Reynolds numbers. A different analysis and further studies should be carried out to investigate the effectiveness of the scheme in spatially developing boundary layers. More positive results could in fact be obtained for open flows since the vortices would not be confined and the fluid pushed towards the wall would come from an undisturbed region void of turbulent small scales.

Comparing the drag reduction mechanism of the current method with two of the more established methods from the literature, i.e., the oscillating walls (see, e.g., Quadrio *et al.* [5]) and the spanwise traveling waves by volume forcing (Du and Karniadakis [28]) at least qualitative similarities can be pointed out. In all of these cases there is a significant portion of the near-wall region in which the flow experiences a significant spanwise velocity relative to the wall. Even though the amplitudes of this spanwise component are different, and inertial effects do not allow for a direct comparison, the implied modifications of the flow appear to be similar (see Du and Karniadakis [28]), i.e., a distortion of the regeneration process. A more quantitative comparison of these methods, and their effect on the near-wall flow, could constitute a further step towards effective flow control.

Financial support by the Swedish Research Council (VR) is gratefully acknowledged. Computer time was provided by the Swedish National Infrastructure for Computing (SNIC). P.S. acknowledges

financial support by the Wallenberg Foundation as part of the Wallenberg Academy Fellow Programme, and R.Ö. acknowledges support from the Lundeqvist Foundation.

[1] M. Gad-el Hak, *Flow Control: Passive, Active, and Reactive Flow Management* (Cambridge University Press, Cambridge, UK, 2007).
[2] R. García-Mayoral and J. Jiménez, Drag reduction by riblets, Phil. Trans. R. Soc. A **369**, 1412 (2011).
[3] T. Min, S. M. Kang, J. L. Speyer, and J. Kim, Sustained sub-laminar drag in a fully developed channel flow, J. Fluid Mech. **558**, 309 (2006).
[4] H. Mamori, K. Iwamoto, and A. Murata, Effect of the parameters of traveling waves created by blowing and suction on the relaminarization phenomena in fully developed turbulent channel flow, Phys. Fluids **26**, 015101 (2014).
[5] M. Quadrio, P. Ricco, and C. Viotti, Streamwise-traveling waves of spanwise wall velocity for turbulent drag reduction, J. Fluid Mech. **627**, 161 (2009).
[6] R. Nakanishi, H. Mamori, and K. Fukagata, Relaminarization of turbulent channel flow using traveling wave-like wall deformation, Int. J. Heat Fluid Flow **35**, 152 (2012).
[7] M. Mishra and M. Skote, Drag reduction in turbulent boundary layers with half wave wall oscillations, Math. Probl. Eng. **2015**, 253249 (2015).
[8] M. Skote, Scaling of the velocity profile in strongly drag reduced turbulent flows over an oscillating wall, Int. J. Heat Fluid Flow **50**, 352 (2014).
[9] Y. Kametani, K. Fukagata, R. Örlü, and P. Schlatter, Effect of uniform blowing/suction in a turbulent boundary layer at moderate Reynolds number, Int. J. Heat Fluid Flow **55**, 132 (2015).
[10] E. Moreau, Airflow control by non-thermal plasma actuators, J. Phys. D. Appl. Phys. **40**, 605 (2007).
[11] W. Schoppa and F. Hussain, A large-scale control strategy for drag reduction in turbulent boundary layers, Phys. Fluids **10**, 1049 (1998).
[12] K. Iwamoto, Y. Suzuki, and N. Kasagi, Reynolds number effect on wall turbulence: Toward effective feedback control, Int. J. Heat Fluid Flow **23**, 678 (2002).
[13] E. Hurst, Q. Yang, and Y. M. Chung, The effect of Reynolds number on turbulent drag reduction by streamwise travelling waves, J. Fluid Mech. **759**, 28 (2014).
[14] D. Gatti and M. Quadrio, Reynolds-dependence of turbulent skin-friction drag reduction induced by spanwise forcing, J. Fluid Mech. **802**, 553 (2016).
[15] J. Canton, R. Örlü, C. Chin, N. Hutchins, J. Monty, and P. Schlatter, On large-scale friction control in turbulent wall flow in low Reynolds number channels, Flow, Turbul. Combust. **97**, 811 (2016).
[16] N. Kasagi, Y. Suzuki, and K. Fukagata, Microelectromechanical systems-based feedback control of turbulence for skin friction reduction, Annu. Rev. Fluid Mech. **41**, 231 (2009).
[17] S. J. Kline, W. C. Reynolds, F. A. Schraub, and P. W. Runstadler, The structure of turbulent boundary layers, J. Fluid Mech. **30**, 741 (1967).
[18] R. D. Moser, J. Kim, and N. N. Mansour, Direct numerical simulation of turbulent channel flow up to $\mathrm{Re}_\tau = 590$, Phys. Fluids **11**, 943 (1999).
[19] D. Gatti and M. Quadrio, Performance losses of drag-reducing spanwise forcing at moderate values of the Reynolds number, Phys. Fluids **25**, 125109 (2013).
[20] M. Chevalier, P. Schlatter, A. Lundbladh, and D. S. Henningson, SIMSON: A pseudo-spectral solver for incompressible boundary layer flows, KTH Mechanics, Stockholm, Sweden, 2007, Tech. Rep., TRITA-MECH 2007:07.
[21] N. Hutchins and K.-S. Choi, Experimental investigation of turbulence suppression by the imposition of a large-scale vortical control flow, in *15th AIAA Computational Fluid Dynamics Conference* (American Institute of Aeronautics and Astronautics, Reston, VA, 2001).
[22] C. Vanderwel and B. Ganapathisubramani, Effects of spanwise spacing on large-scale secondary flows in rough-wall turbulent boundary layers, J. Fluid Mech. **774**, R2 (2015).
[23] O. J. E. Matsson and P. H. Alfredsson, Curvature- and rotation-induced instabilities in channel flow, J. Fluid Mech. **210**, 537 (1990).

[24] K.-S. Choi, T. Jukes, and R. Whalley, Turbulent boundary-layer control with plasma actuators, Phil. Trans. R. Soc. A **369**, 1443 (2011).

[25] M. Wicks, F. O. Thomas, T. C. Corke, M. Patel, and A. B. Cain, Mechanism of vorticity generation in plasma streamwise vortex generators, AIAA J. **53**, 3404 (2015).

[26] C. Tropea, A. L. Yarin, and J. F. Foss, *Springer Handbook of Experimental Fluid Mechanics* (Springer Science & Business Media, Berlin, 2007).

[27] K. Fukagata, M. Kobayashi, and N. Kasagi, On the friction drag reduction effect by a control of large-scale turbulent structures, J. Fluid Sci. Technol. **5**, 574 (2010).

[28] Y. Du and G. E. Karniadakis, Suppressing wall turbulence by means of a transverse traveling wave, Science **288**, 1230 (2000).